IEEE Access
Multidisciplinary | Rapid Review | Open Access Journal

Received 10 January 2024, accepted 13 February 2024, date of publication 19 February 2024, date of current version 23 February 2024.

Digital Object Identifier 10.1109/ACCESS.2024.3367011

RESEARCH ARTICLE

Automatic Generation Control of a Hybrid PV-Reheat Thermal Power System Using RIME Algorithm

SERDAR EKINCI[1], ÖZAY CAN[2], MUSTAFA ŞINASI AYAS[3], (Member, IEEE), DAVUT IZCI[1], MOHAMMAD SALMAN[4], (Senior Member, IEEE), AND MOSTAFA RASHDAN[4], (Senior Member, IEEE)

[1]Department of Computer Engineering, Batman University, 72100 Batman, Turkey
[2]Department of Electronics and Automation, Recep Tayyip Erdogan University, 53100 Rize, Turkey
[3]Department of Electrical Electronics Engineering, Karadeniz Technical University, 61080 Trabzon, Turkey
[4]College of Engineering and Technology, American University of the Middle East, Egaila 54200, Kuwait

Corresponding author: Mohammad Salman (mohammad.salman@aum.edu.kw)

ABSTRACT This study focuses on the automatic generation control (AGC) system, which is crucial for maintaining balance between power generation and demand in power systems. The implementation of the AGC system needs to be more precise due to the increasing uncertainty surrounding renewable energy sources (RESs) and changes in demand. The objective of this study is to investigate the AGC functions in a two-area hybrid power system that combines a PV system with a reheat thermal system. To improve system performance, we utilize a proportional-integral (PI) controller. We utilized a recently developed optimization method, RIME, for tuning controller parameters. This technique has not been studied before in AGC processes. Furthermore, the optimization procedure utilizes a modified version of the integral of time-multiplied absolute error (ITAE) objective function. The study compares the performance of the RIME-tuned PI controller under various scenarios, including changes in thermal system load, load variations in both areas, and robustness considerations, with well-known techniques in the literature, such as the black widow optimization algorithm (BWOA), the salp swarm algorithm (SSA), the shuffled frog leaping algorithm (SFLA), the firefly algorithm (FA) and the genetic algorithm (GA). Our comparative study demonstrates that the proposed controller outperforms state-of-the-art approaches in terms of overshoot values and damping durations for both system frequency and tie-line power changes. The study provides valuable information on the effectiveness of the RIME-tuned PI controller in controlling AGC processes in complex hybrid power systems.

INDEX TERMS Automatic generation control, RIME algorithm, hybrid PV-reheat thermal system, ITAE, frequency deviation.

I. INTRODUCTION

Power systems are intricate infrastructures composed of various components, each with distinct load capacities. In the dynamic realm of modern power distribution, ensuring a steady and abundant energy supply is crucial. This need arises from the dynamic nature of power systems, where variations in power generation relative to load demand induce frequency fluctuations. Left uncontrolled, these variations can lead to undesirable outcomes, including power system failures. To address this, Automatic Generation Control (AGC) is indispensable for coordinating electric power systems. AGC's primary function is to meticulously control tie line power and system frequency variation, ensuring adherence to predetermined limits [1], [2], thereby safeguarding power system stability and reliability against the adverse effects of frequency oscillations.

As conventional energy sources deplete, renewable energy sources (RES) gain prominence. Integrating RES, particularly photovoltaic (PV) systems, into power generation is

The associate editor coordinating the review of this manuscript and approving it for publication was Ahmed F. Zobaa.

challenging due to their intermittent nature. PV systems offer benefits such as reduced maintenance costs and suitability for distributed power generation. However, solar energy's intermittency requires the incorporation of numerous battery systems for consistent and reliable power output [1], [2], [3], [4]. Integrating traditional energy sources like thermal generators with RES seems practical, optimizing benefits while providing a steady power output. However, the addition of PV systems introduces fluctuations, necessitating precise AGC timing, especially in hybrid systems with frequency oscillations triggered by PV output intermittency [3], [4].

In research incorporating RES into AGC systems, a prevalent pattern is the use of simplified first-order models to represent RES transfer functions [5], [6], [7]. While these models capture fundamental dynamics, they oversimplify the complexity of RES, particularly PV systems. Existing literature often overlooks the structural subtleties of PV systems, including fluctuating solar irradiance, nonlinearities in power conversion, and environmental influences, potentially limiting AGC model accuracy [5], [6], [7].

Beyond the traditional proportional-integral (PI) controllers [1], [2], [3], [4], a number of controllers are emerging in the complex field of AGC for power systems integrating RES. The exploration of advanced control strategies includes fractional-order PI (FOPI) [8], which introduces a nuanced fractional calculus element, proportional-integral-derivative (PID) [9], which provides enhanced dynamics, FOPID [10], which integrates fractional calculus for improved tuning flexibility, and fractional order fuzzy PID (FOFPID) [11], which fuses fuzzy logic with fractional-order dynamics for a more adaptive and robust control paradigm. The critical role these controllers play in influencing power system response highlights the importance of accurately setting their parameters. An important factor affecting the overall performance of the AGC process is the optimization of these parameters. To achieve this, researchers have studied a wide range of optimization techniques, each designed to optimize controller settings and improve system performance.

Various optimization algorithms have been explored in these studies, each with their unique inspiration. For instance, the grasshopper optimization algorithm (GOA) [12] imitates the swarming behavior of grasshoppers, while the dragonfly search algorithm (DSA) [13], [14], [15] replicates the foraging behavior of dragonflies. Additionally, the jellyfish search optimizer (JSO) [10] simulates the pulsating motion of jellyfish. Moving beyond, the whale optimization algorithm (WOA) [16] draws inspiration from the social behavior of humpback whales, and the grey wolf optimization algorithm (GWO) [17] mimics the hunting techniques of gray wolves. Further diversifying the optimization approaches are the elephant herding optimization (EHO) [18], emulating the herding behavior of elephants, and the jaya algorithm (JA) [19], driven by the concept of communal optimization. This array of optimization methods creates a dynamic and diverse landscape of algorithms, each specifically advantageous in capturing the intricate dynamics resulting from the integration of RES into power systems. In the context of hybrid power systems, selecting an optimization technique becomes a critical decision point to ensure the flexibility, effectiveness, and robustness of the AGC process.

Developing an objective function (OF) is also a crucial step in the intricate field of AGC optimization, as it profoundly influences the reduction of system frequency oscillations and tie line power fluctuations. Optimization aims to achieve a delicate balance between power generation and demand, with the selection of a suitable OF serving as a guiding metric. The research delves into various performance metrics, each attempting to capture specific aspects of the AGC process and system behavior. One prominent traditional metric is the integral of the square of the error (ISE) [7], [20], which calculates the cumulative squared deviations between the actual and desired system responses. Another perspective is offered by the integral of the absolute error (IAE) [5], emphasizing accumulated absolute deviations and providing a measure of the overall error magnitude. Expanding the study's scope is the integral of the square of the time-weighted error (ITSE) [21], introducing a temporal dimension to reflect the changing dynamics of the power system by assigning different weights to errors at distinct time instances. Further broadening the range of performance indices is the integral of time-weighted absolute error (ITAE) [22], [23], combining the elements of IAE with temporal weighting to offer a complex view of the time-dependent aspects of system performance. Each of these indices provides a unique perspective on various facets of system stability and reactivity, serving as valuable tools for evaluating AGC efficiency.

This study focuses on enhancing the realism of AGC procedures through a comprehensive review of existing literature. The aim is to establish a more equitable basis for comparison with prior research. To achieve this, the research employs a novel approach by investigating the dynamics of an interconnected hybrid power system encompassing two areas. This system combines conventional and renewable energy sources, specifically a thermal power system and a PV system. The inclusion of both PV and thermal components introduces a level of complexity and realism in line with the evolution of modern power systems.

In the context of AGC in hybrid power systems, PI controllers are commonly preferred due to extensive prior study. In this research, the PI controller is chosen as the control mechanism, aligning with established approaches in previous studies. However, a distinctive aspect of this research lies in the application of a novel optimization method called RIME algorithm [24]. Notably, RIME has never been utilized in the AGC process for PV thermal power systems. This unique perspective aims to evaluate the performance of the PI controller when optimized using this state-of-the-art approach.

A detailed comparison of various studies reveals that the ITAE is frequently used as the OF. Despite its common usage, observed discrepancies in system frequency oscillations and

tie line power variation prompt a proactive adjustment of the ITAE in this study. This modification seeks to enhance the precision and reliability of the AGC procedure in the considered hybrid power system.

Furthermore, the research conducts an extensive robustness analysis to fortify the validity of its conclusions. The robustness of the system is rigorously tested against various objective functions, underscoring the study's commitment to a comprehensive investigation of the proposed AGC framework. The ultimate goal of this work is to contribute to the advancement of knowledge in AGC, establishing a standard for evaluating hybrid power systems. This standard considers real-world dynamics and pushes the boundaries of controller tuning optimization methods. The followings are a summary of the distinctive contributions of this study:

- Investigating the dynamics of an interconnected hybrid power system, which consists of two areas and seamlessly combines a PV and a thermal power system.
- Introducing the use of recently developed RIME optimization in AGC process. This technique has never been applied to the AGC process in PV thermal power systems.
- Using a modified ITAE objective function in order to address the observed differences in tie line power variation and system frequency oscillations reported in the literature. This adjustment improves the accuracy and reliability of the AGC process, which also improves the system performance.
- Performing a thorough comparison with the latest research in the field to demonstrate the robustness of the proposed approach.

The rest of the paper is organized as follows: Section II thoroughly examines the RIME algorithm, providing insight into its operation and underlying ideas. Section III delves into the power system concept and provides a comprehensive overview of the interconnected hybrid system using AGC. The reader's understanding is enhanced by Section IV's insights into the optimization problem at the heart of the research. Section V presents the simulation results and noteworthy conclusions, highlighting the performance of the AGC framework in both quantitative and qualitative dimensions. Finally, the paper is summarized in Section VI, which also provides conclusions and implications based on the results of the study.

II. RIME ALGORITHM

The RIME algorithm, described in detail by Su et al. in their work [24], [25], serves as a pivotal optimization method in this study. It is inspired by the hoar-frost ice evolution process and is structured into four phases.

A. RIME CLUSTER INITIALIZATION

The RIME algorithm begins by initializing a population (denoted as X) of search agents based on the characteristics of hoar-frost ice evolution. The initialization is performed by (1) where D represents the size of the problem.

$$X = \begin{bmatrix} x_{11} & x_{12} & \dots & x_{1D} \\ x_{21} & x_{22} & \dots & x_{2D} \\ \vdots & \vdots & \ddots & \vdots \\ x_{N1} & x_{N2} & \dots & x_{ND} \end{bmatrix} \tag{1}$$

These agents form the foundation for subsequent operations. The RIME algorithm employs a soft-rime search strategy, characterized by targeted randomization to overcome local stagnation. In that sense, the definition in (2) is employed for $r_2 < E$:

$$R_{ij}^{new} = R_{best,j} + Rf \times \left(h \times \left(B_{max(i,j)} - B_{min(i,j)}\right) + B_{min(i,j)}\right) \tag{2}$$

where $Rf = r_1 \times cos\theta \times \beta$, $\theta = \pi \cdot (t\,(10 \cdot T))$, $\beta = 1 - ((w \cdot t/T)/w)$ and $E = \sqrt{(t/T)}$. Here, $R_{best,j}$ identifies the most effective RIME agent in the RIME population. The position of the free particle after the motion is denoted by R_{ij}^{new} and r_1 is a random number ranging from -1 and 1. The value of $cos\theta$ increases proportionally with the algorithm's iteration count. The environment's ambient conditions are represented by β, which varies as the algorithm iterates. The random number h, ranging from 0 to 1, simulates the distance between free particles. The maximum iteration count is represented by T, while t represents the iteration count of the algorithm. w determines the number of segments in the step function, while E indicates the likelihood of collecting free particles. The dynamic approach in this mechanism aims to balance exploration and exploitation, preventing premature convergence to suboptimal solutions.

The hard-rime puncture mechanism, inspired by the natural breaking of hoarfrost, introduces perturbations among search agents. This disturbance is essential for avoiding local optima and enhancing the convergence of the algorithm. This mechanism is mathematically defined as given in (3):

$$R_{ij}^{new} = R_{best,j}, r_3 < F^{normr}(S_i) \tag{3}$$

where R_{ij}^{new} is the j^{th} particle of the population's best fracking agent, and $R_{best,j}$ is the updated particle position.

The fitness value of the current agent is normalized to obtain $F^{normr}(S_i)$. Here, r_3 is a random number between -1 and 1, and $F^{normr}(S_i)$ represents the probability of the agent experiencing a hard puncture.

The optimization process includes positive greedy selection, systematically comparing modified search agents' fitness values to update them if improvements are detected. This iterative improvement raises the overall standard of search agents over time. The pseudocode, given in Algorithm 1, outlines the RIME algorithm.

III. SYSTEM MODELING

The power system chosen for the AGC investigation in this study is a sophisticated two-area hybrid configuration. A PV system and a reheat thermal power subsystem collaboratively constitute this system. In the distribution layout, the PV

Algorithm 1 Pseudocode of RIME Algorithm

Set the RIME population to start.
Find the best agent and the corresponding fitness score.
While $t \leq T$
  $E = (t/T)^0.5$
  If $r_2 < E$
    Use **the soft-RIME search strategy** to update the RIME agent's position.
  End If
  If $r_3 <$ *Normalize fitness of* S_i
    Utilizing **the hard rime puncture mechanism**, carry out a cross-agency update.
End If
If $F(R_i^{new}) < F(R_i)$
    Determine which is the best solution using **positive greedy selection**.
  End If
  $t = t + 1$
End While

system and associated loads are positioned in Area-1, while the reheat thermal power system is located in Area-2. Figure 1 illustrates a schematic diagram of the AGC process for this two-area thermal power system.

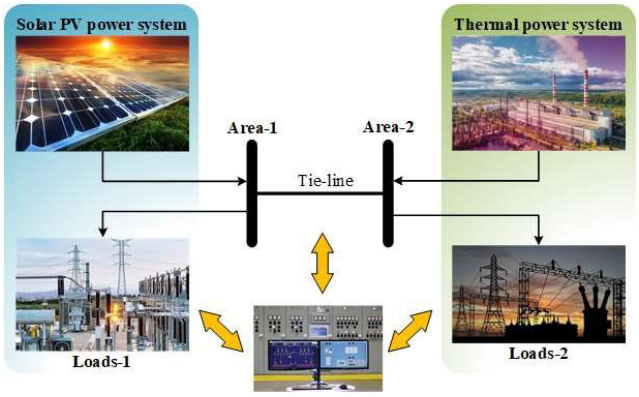

FIGURE 1. Schematic diagram of power system.

Since external variables can introduce unpredictability into voltage values obtained from PV panels, relying solely on PV panels as the energy source can pose challenges. These challenges may include frequency oscillations due to difficulties in meeting load requirements. Traditional approaches to address these issues involve working in conjunction with an alternative energy source or integrating energy storage devices, such as batteries. This study takes a unique approach by closely integrating the PV system with the thermal power supply, rather than depending on batteries. The purpose of this interconnection is to facilitate a seamless transfer of energy between the PV and thermal systems, enabling them to collaboratively meet diverse load demands without relying on battery storage. This innovative setup not only mitigates the intermittent nature of PV energy but also fosters a dynamic interplay between the PV and thermal subsystems. Because of their interdependence, these two energy sources can respond to load demands in a coordinated manner, minimizing the challenges faced by standalone PV systems and enhancing the overall efficiency of the hybrid power system.

A. MODELING OF THERMAL POWER SYSTEM

The thermal power system in Area 2 comprises four complex components: the governor, turbine, reheater, and power system. Adopting a practical approach, we develop a transfer function model for the power system by treating all components as linear entities and representing them with first-order transfer functions. The description of the transfer functions governing each thermal system component can be found in [1], [2], [3], and [4] and briefly described as follows. The transfer function of the governor is given in (4) where K_g is the governor gain and τ_g is the governor time constant.

$$G_g(s) = \frac{K_g}{s\tau_g + 1} \tag{4}$$

The transfer function of the turbine is given in (5) where K_t is the turbine gain and τ_t is the turbine time constant.

$$G_t(s) = \frac{K_t}{s\tau_t + 1} \tag{5}$$

The reheater transfer function is given in (6) where K_r is the reheater gain and τ_r is the reheater time constant.

$$G_r(s) = \frac{sK_r\tau_r + 1}{s\tau_r + 1} \tag{6}$$

The transfer function of the power system in Area 2 is defined in (7) where K_{ps} is the power system gain and τ_{ps} is the power system time constant.

$$G_{ps}(s) = \frac{K_{ps}}{s\tau_{ps} + 1} \tag{7}$$

In addition, (8) is used to calculate the area control error (ACE) for the i^{th} area by taking into account important variables such as the frequency bias parameter (B), the frequency deviation of the i^{th} area (Δf_i) and the variance of the tie line power across the areas (ΔP_{tie}).

$$ACE_i = B\Delta f_i + \Delta P_{tie} \tag{8}$$

B. MODELING OF PHOTOVOLTAIC SYSTEM

The initial step in accurately simulating a PV system involves modeling a solar cell. The circuit design in Figure 2 presents an analog model of a solar cell, comprising a series resistor, a coupled p-n diode, and a PV current source. Solar energy is introduced into the circuit through this PV current source, generating current that is influenced by solar radiation and is temperature and irradiance dependent. To optimize the energy harvested from the solar panel in varying external conditions, Maximum Power Point Tracking (MPPT) is crucial. By adapting to changing conditions, the

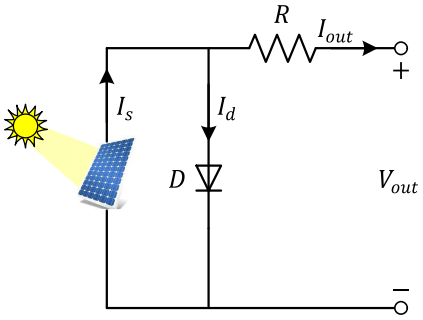

FIGURE 2. Equivalent circuit of solar cell.

MPPT mechanism ensures the system operates at its peak efficiency. As solar panels naturally collect energy in DC form, conversion to AC is necessary for compatibility with standard loads. Inverters play a vital role in converting DC power into AC power, enabling the utilization of solar panel output by AC loads.

Considering these aspects, the transfer function of the PV system, encompassing MPPT, converters, and filters, is accurately described in (9).

$$G_{PV}(s) = \frac{-18s + 900}{s^2 + 100s + 50} \tag{9}$$

Building upon the previously described transfer functions, Figure 3 graphically illustrates the transfer function model of the two-area hybrid power system. To enhance transparency and provide a reference point for future simulations and studies, the values of $K_{ps} = 120Hz/pu.MW$, $\tau_{ps} = 20s$, $K_r = 0.33Hz/pu.MW$, $2\pi T_{12} = 0.545pu.MW/Hz$, $\tau_r = 10s$, $\tau_g = 0.08s$, $\tau_t = 0.3s$, $B = 0.8pu.MW/Hz$ and $R = 2.5Hz/pu.MW$ are adopted in this study.

IV. DEFINITION OF OPTIMIZATION PROBLEM AND PROPOSED DESIGN METHOD

The power generated by the control regions meets the current load demand under normal operating conditions. However, in specific scenarios, additional load demand may surpass the system's capacity, leading to a mismatch between the power generated and required power. This mismatch induces oscillations in the system frequency and tie line power, causing instability in the power grid. The primary objective of the AGC procedure is to swiftly mitigate these oscillations, either eliminating them entirely or keeping them within preset tolerance limits. This goal is achieved through the deployment of controllers. In this work, a PI controller, a widely used and reputable control mechanism, is employed. Its effectiveness has been demonstrated in numerous comparative studies. The transfer function for a system with n-areas are provided in (10) where K_{pn} is the proportional gain of the n^{th} area and K_{in} is the integral gain of the n^{th} area.

$$G_{Cn}(s) = K_{pn} + \frac{K_{in}}{s} \tag{10}$$

The power system assigned to AGC in this study operates within a two-area structure. The optimization process relies on four essential parameters, namely K_{p1}, K_{i1}, K_{p2}, and K_{i2}. These parameters play a crucial role in determining the performance of the AGC system. Therefore, optimizing them is necessary to achieve the best possible control and reaction. The AGC procedure aims to minimize crucial time-domain features such as settling time (ST), undershoot (US), and overshoot (OS) by determining control settings. These features directly impact the system's capacity to react quickly and precisely to variations in power consumption, thereby maintaining stability and reducing oscillations. While control parameters can be decided through trial and error, this method is often ineffective and time-consuming. Therefore, it is essential to approach the parameter determination procedure as an optimization issue.

The main goal of optimization is to find solutions that fall within a suitable parameter space by minimizing a specified objective function (OF). This study employs integral of time-weighted absolute error (ITAE) as the OF for optimization, consistent with similar works in the field. The ITAE OF is a comprehensive measure of the system's performance over time and aligns with the overarching objective of attaining stable and effective AGC in the two-area power system. The transfer function of the OF is given in (11).

$$OF_{ITAE} = \int_0^{t_f} t \cdot (|\Delta f_1| + |\Delta f_2| + |\Delta P_{tie}|) \cdot dt \tag{11}$$

In the equation, t represents the current time, and t_f denotes the simulation duration, which is set to 50 seconds. Additionally, the constraints of $-2 \leq K_{p1}, K_{i1}, K_{p2}, K_{i2} \leq 2$ have been considered during the optimization process.

A noteworthy finding from comparative research was that variations in tie line power and system frequency oscillations tended to exceed certain thresholds. To efficiently attenuate and regulate these aberrations, an ITAE objective function has been added. This enhancement aims to limit overshoot values from exceeding predefined thresholds, ensuring more stable operation within the given parameters. The ITAE objective function acts as a safety net, keeping the system's reaction dynamics within allowable bounds and promoting a more effective AGC process by accounting for these restrictions during the optimization process.

- $|\Delta f_1| \leq 0.25$; $|\Delta f_2| \leq 0.25$; $|\Delta P_{tie}| \leq 0.05$

Figure 4 displays the schematic diagram of the AGC process using the innovative RIME algorithm in a two-area PV-thermal power system. The modeling procedure begins by constructing a power system model using Matlab/Simulink. The created model is then seamlessly linked with the written codes of the RIME method found in the m-file. To introduce some degree of unpredictability into the system, four parameters (two for each controller in both areas) are stochastically determined. The Simulink model utilizes the aforementioned parameter values to monitor and analyze dynamic fluctuations in tie line power and

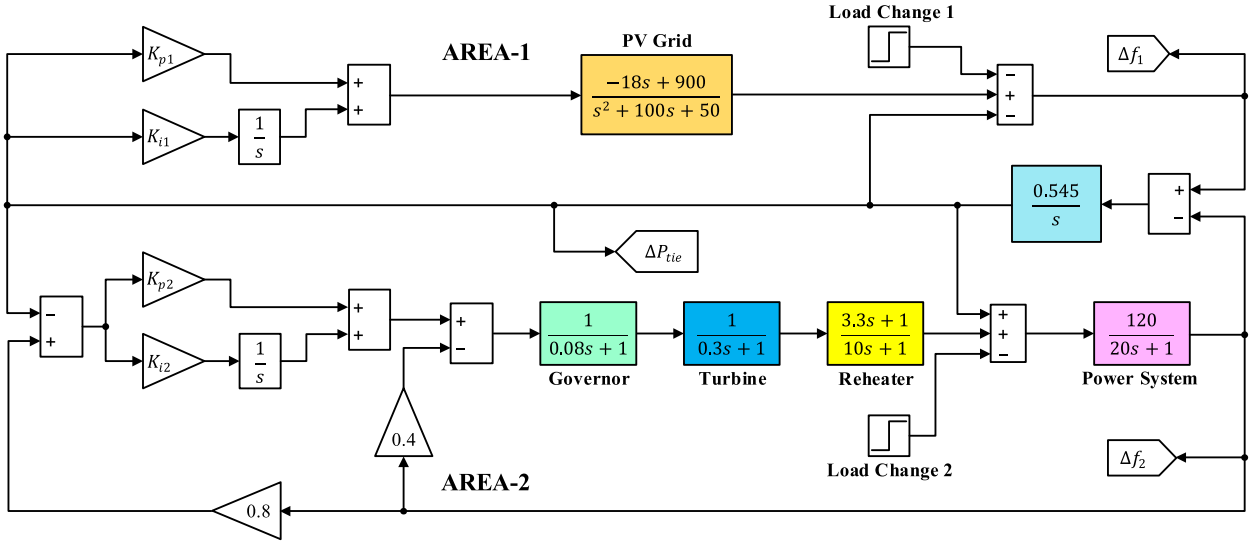

FIGURE 3. Overall two-area hybrid system.

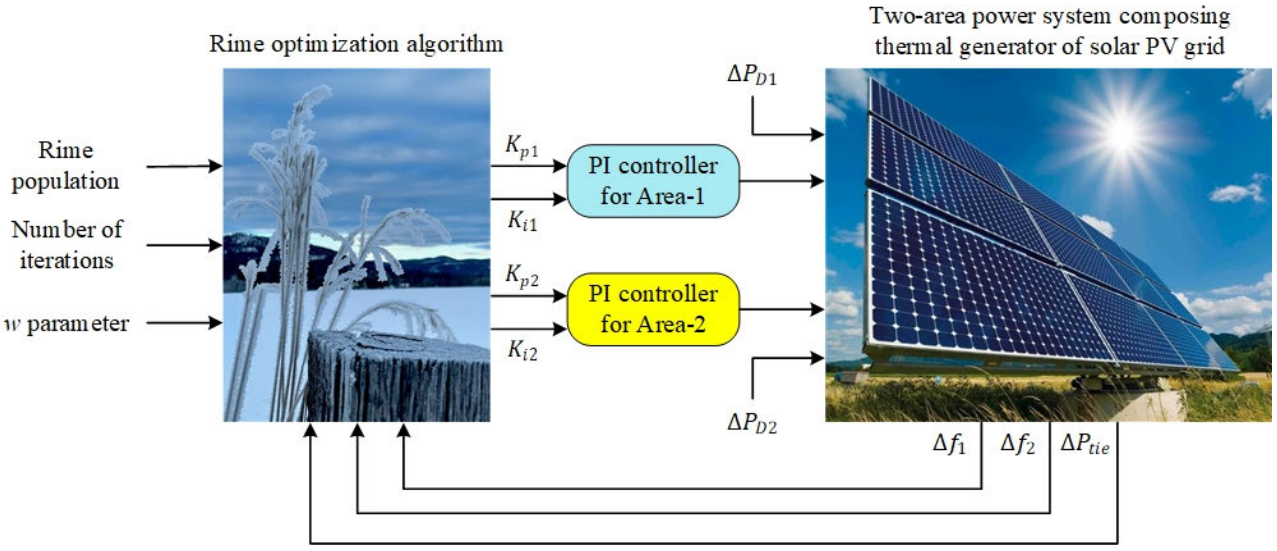

FIGURE 4. Application of RIME algorithm to two-area power system.

frequency. The obtained values are then used as inputs to calculate the increased *OF*, representing the system's performance under the given parameter set. The optimization process undergoes an additional cycle using the computed values. This process refines the settings to enhance the performance of the AGC system, achieving optimal stability and response characteristics. This iterative loop continues until the predefined stopping requirements are met.

V. SIMULATION RESULTS AND DISCUSSION

This section of the research provides a comprehensive analysis of the performance of the RIME-tuned PI controller in three different scenarios. Firstly, the system's response to a 0.1 *pu* load change that occurs in the thermal system at 0*s* is examined in detail. This case study highlights the controller's ability to handle sudden changes and maintain system stability. After that, a more complicated situation is presented in which both areas experience a simultaneous 0.1 *pu* load change at 0*s*. This situation emulates a more challenging real-world circumstance, enabling an evaluation of the controller's ability to coordinate responses among different hybrid power system components. Finally, the robustness of the proposed RIME-tuned PI controller is assessed under different objective functions. These scenarios offer a thorough assessment of the controller's robustness and performance under various operating settings.

A. STATISTICAL ANALYSIS

The optimization procedure is carried out in the Matlab/Simulink environment. The procedure consisted of

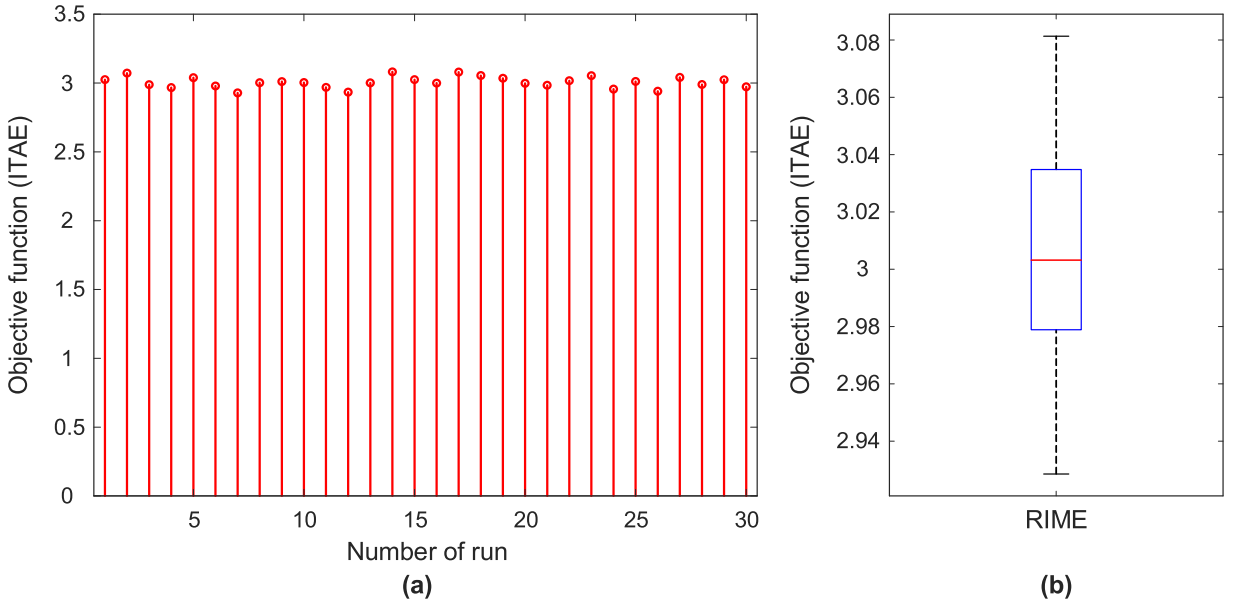

FIGURE 5. Obtained ITAE values for 30 runs (a) and Boxplot analysis (b).

30 runs with a population size of 50 and 50 iterations overall. Figure 5 shows the values of the *OF* for each run in a boxplot graph.

The figure depicts the distribution of ITAE values over the 30 runs, providing information on the optimization results' variability. A statistical analysis was conducted on the ITAE values, including characteristics such as minimum, maximum, median, average, and standard deviation, to provide a comprehensive explanation of the obtained data. Table 1 presents a detailed summary of the statistics. Figure 5 and Table 1 show that the average ITAE value varied over the 30 runs, ranging from 2.9285 to 3.0814. The average ITAE score overall is approximately 3, indicating consistent performance during the optimization process.

TABLE 1. Statistical metrics of objective function.

Minimum	Maximum	Median	Average	Standard deviation
2.9285	3.0814	3.0032	3.0062	0.040876

B. CHANGES OF CONTROLLER PARAMETERS AND ITAE OBJECTIVE FUNCTION

Figure 6 displays the convergence behavior of the RIME method when applied to the ITAE objective function. The graph depicts the convergence curve after 50 iterations. Upon close examination of Figure 6, a clear trend emerges. The *OF* displays a dynamic pattern of convergence, gradually approaching and stabilizing at a value of approximately 3. It is intriguing to note that this convergence towards the optimal value is visible from the 15^{th} iteration onwards.

The variation of the controller parameters along the determined iteration is shown in Figure 7. As can be seen from Figure 7, all four controller parameters converge to

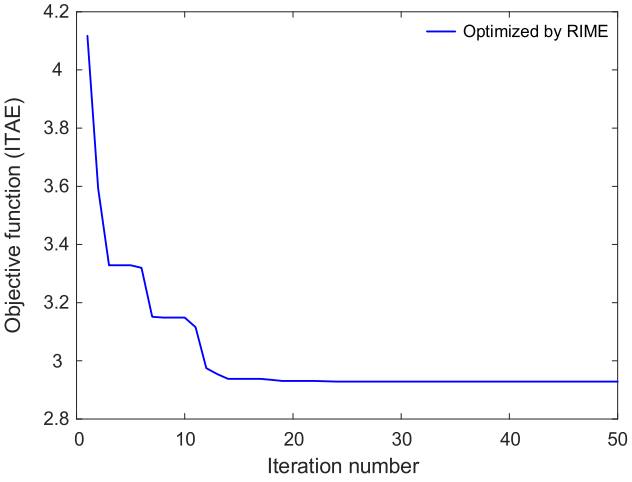

FIGURE 6. Evolution curve for ITAE.

their final values given in Table 2 after a certain iteration as expected.

TABLE 2. Optimized PI controller parameters.

Approach	K_{p1}	K_{i1}	K_{p2}	K_{i2}
RIME-tuned PI (proposed)	−0.45397	−0.093464	−2	−0.94357
BWOA-tuned PI [1]	−0.66708	−0.54768	−2	−0.84696
SSA-tuned PI [2]	−0.7715	−0.0483	−1.0837	−0.8929
SFLA-tuned PI [3]	−0.5156	−0.9012	−0.7896	−0.8965
FA-tuned PI [4]	−0.8811	−0.5765	−0.7626	−0.8307
GA-tuned PI [4]	−0.5663	−0.4024	−0.5127	−0.7256

C. COMPARED RECENT APPROACHES

The optimum controller parameters obtained after 30 runs for 50 iterations using the RIME algorithm and the controller parameters proposed in BWOA-tuned PI [1], SSA-tuned

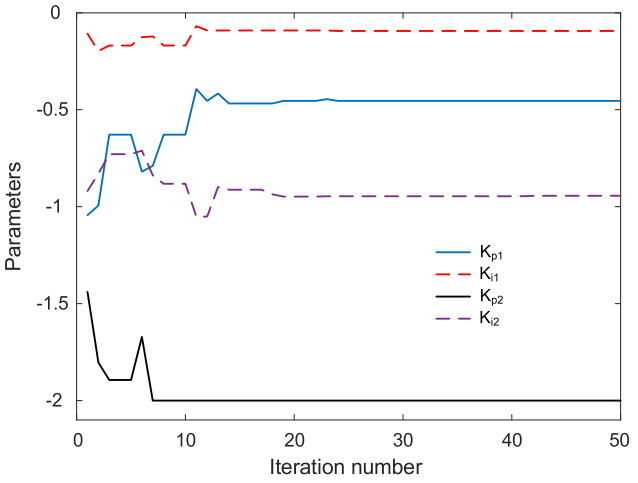

FIGURE 7. Evolution curves for controller parameters.

PI [2], SFLA-tuned PI [3], FA-tuned PI [4] and GA-tuned PI [4] are given in Table 2.

D. CASE STUDIES

Performance indices such as ST (± 0.1 Hz tolerance band for Δf_1 and Δf_2 and ± 0.025 MW tolerance band for ΔP_{tie}), OS and US are considered while analysing the performance of the RIME-tuned PI controller used in the two-area hybrid PV-thermal power system under different scenarios.

1) DISTURBANCE (A)

In this case study (10% step change ($\Delta P_{D1} = 0.1$ pu) in thermal system demand), the system behavior under load change of 0.1 pu at 0s in the second area is investigated. In this context, the frequency variation (Δf_1) in Area-1, frequency variation (Δf_2) in Area-2 and tie line power variation (ΔP_{tie}) graphs are given in Figure 8, Figure 9, and Figure 10, respectively.

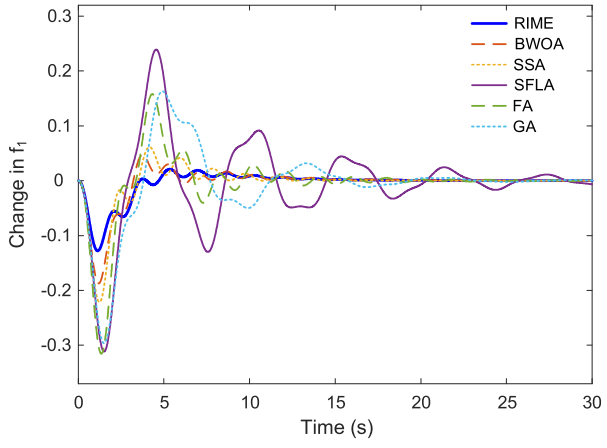

FIGURE 8. Variation in Δf_1 for disturbance (a).

The numerical data obtained from the graphical representations is meticulously collected and presented in tabular form to facilitate quantitative analysis. Tables 3, 4, and 5 provide comprehensive references, including precise numerical values for the observed frequency and power exchange in Area-1, Area-2, and the tie-line, respectively.

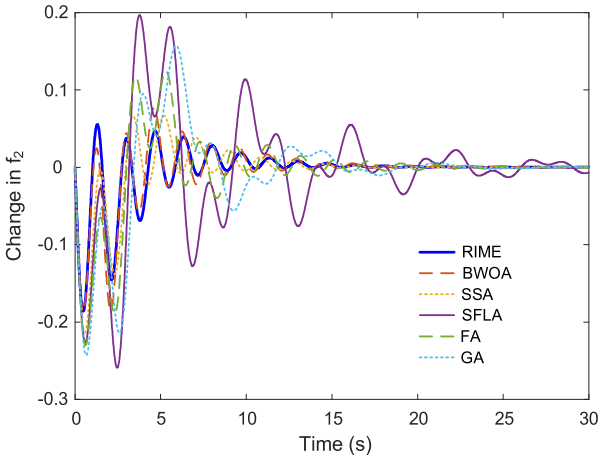

FIGURE 9. Variation in Δf_2 for disturbance (a).

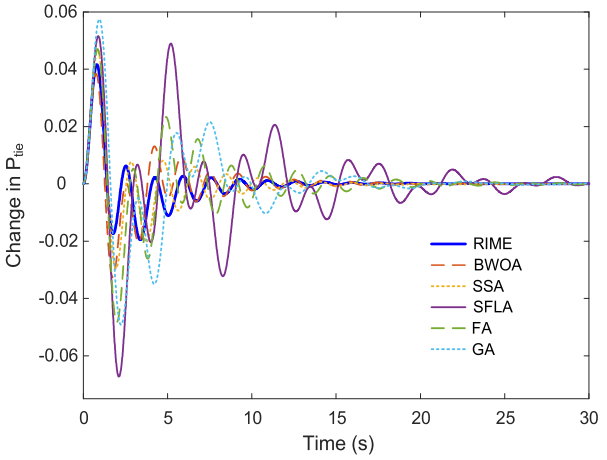

FIGURE 10. Variation in ΔP_{tie} for disturbance (a).

TABLE 3. Numerical results of ST, US and OS for Δf_1 under disturbance (a).

Approach	ST (s)	US	OS
RIME-tuned PI (proposed)	**1.5072**	**−0.12799**	**0.020916**
BWOA-tuned PI [1]	1.8198	−0.18722	0.047009
SSA-tuned PI [2]	1.864	−0.22156	0.061433
SFLA-tuned PI [3]	7.9355	−0.31152	0.23905
FA-tuned PI [4]	4.8247	−0.31541	0.15791
GA-tuned PI [4]	6.6537	−0.29645	0.16298

The performance of the RIME-tuned PI controller is also very impressive, effectively reducing both undershoot and overshoot, as shown in Figure 8 and presented in Table 3. The RIME-tuned PI controller's performance is remarkable in that it outperforms the other tuning strategies by having the shortest settling time, which is 1.5072 s. Examining Table 4, it is evident that the RIME-tuned PI controller remains highly effective. Once again, it outperforms all other controllers, achieving the fastest settling time (2.4135 s). This controller

TABLE 4. Numerical results of *ST*, *US* and *OS* for Δf_2 under disturbance (a).

Approach	*ST* (*s*)	*US*	*OS*
RIME-tuned PI (proposed)	**2.4135**	**−0.18612**	**0.055346**
BWOA-tuned PI [1]	2.4513	−0.18671	0.076656
SSA-tuned PI [2]	2.6092	−0.21499	0.06663
SFLA-tuned PI [3]	10.25	−0.25917	0.19663
FA-tuned PI [4]	5.6017	−0.23017	0.12456
GA-tuned PI [4]	6.4543	−0.24313	0.15741

TABLE 5. Numerical results of *ST*, *US* and *OS* for ΔP_{tie} under disturbance (a).

Approach	*ST* (*s*)	*US*	*OS*
RIME-tuned PI (proposed)	**1.1359**	**−0.019541**	0.041653
BWOA-tuned PI [1]	1.9896	−0.032573	**0.038398**
SSA-tuned PI [2]	2.1262	−0.029649	0.046477
SFLA-tuned PI [3]	8.5916	−0.067258	0.051529
FA-tuned PI [4]	3.9307	−0.048328	0.047025
GA-tuned PI [4]	4.575	−0.049178	0.057467

is capable of minimizing settling time while efficiently controlling overshoot and undershoot. This highlights its ability to maximize Area-2's dynamic response during the defined disturbance scenario. Table 5 provides numerical data on the settling time, undershoot, and overshoot for tie-line power change, offering a comprehensive understanding of the performance of the RIME-tuned PI controller.

The data shows that the RIME-tuned PI controller is the top performer in this domain, with the lowest settling time of 1.1359 s. In addition, its adept management of both undershoot and overshoot demonstrates its efficiency in maintaining a steady power exchange along the tie-line, even when facing designated disturbance conditions.

In conclusion, the RIME-tuned PI controller outperforms the others in all three tables by providing the quickest settling time while simultaneously reducing undershoot and overshoot values. These combined results demonstrate the reliability and efficiency of the RIME-tuned PI controller in coordinating a well-managed system response, particularly in the given disturbance situation.

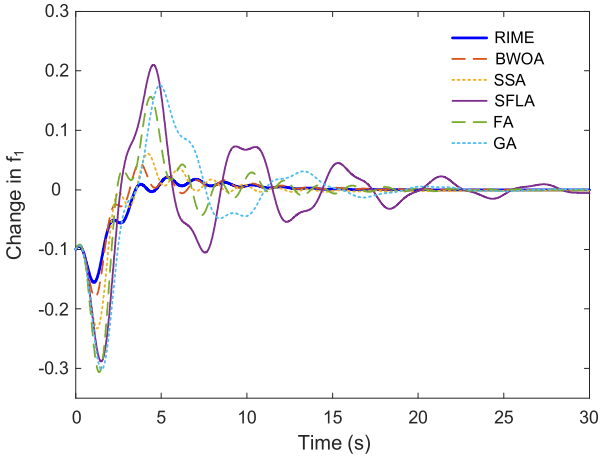

FIGURE 11. Variation in Δf_1 for disturbance (b).

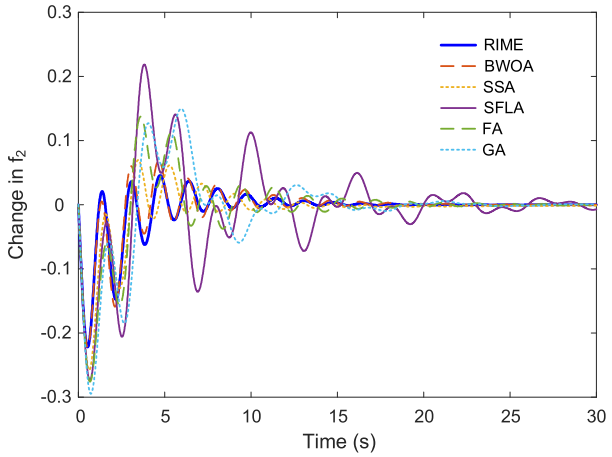

FIGURE 12. Variation in Δf_2 for disturbance (b).

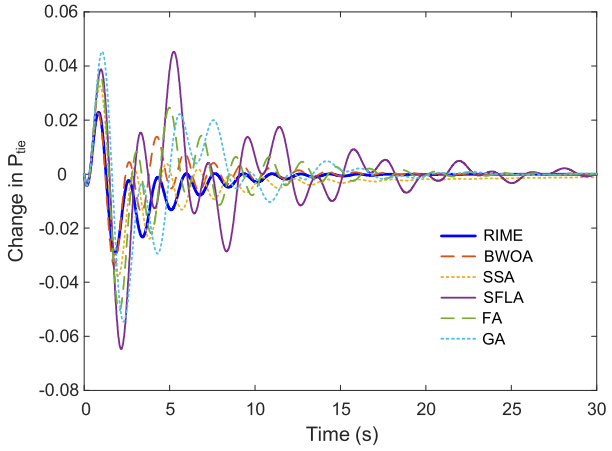

FIGURE 13. Variation in ΔP_{tie} for disturbance (b).

2) DISTURBANCE (B)

This case study (10% step change ($\Delta P_{D1} = 0.1\ pu$ and $\Delta P_{D2} = 0.1\ pu$) in both areas) examines the impact of the PVs on the overall system dynamics. Specifically, we analyze the system's response to a 0.1 *pu* load change that occurs in both system areas at the beginning of the simulation ($0^{th}s$). The resulting change profiles obtained from the simulation studies are presented in Figures 11, 12, and 13, which illustrate the fluctuations in Δf_1, Δf_2, and ΔP_{tie}, respectively. Tables 6, 7, and 8 provide detailed numerical data extracted from the graphical representations. Upon thorough analysis of the figures and tables, it is apparent that the proposed RIME-tuned PI controller significantly mitigates frequency oscillations (Δf_1 and Δf_2,) and tie line power variations (ΔP_{tie}) in a shorter time frame compared to other methods. Additionally, the undershoot and overshoot values remain consistently within the predetermined boundaries established in this study. The findings highlight how quickly and effectively the RIME-tuned PI controller can dampen system oscillations, improving the performance and stability of the frequency and tie line power responses. The

controller's ability to keep undershoot and overshoot values within predetermined limits is particularly noteworthy in the presence of load change, further enhancing its effectiveness in maintaining a controlled and stable system response.

TABLE 6. Numerical results of *ST*, *US* and *OS* for Δf_1 under disturbance (b).

Approach	*ST* (*s*)	*US*	*OS*
RIME-tuned PI (proposed)	**1.6219**	**−0.15529**	**0.02131**
BWOA-tuned PI [1]	1.7001	−0.18025	0.045618
SSA-tuned PI [2]	1.9059	−0.23269	0.061061
SFLA-tuned PI [3]	5.2736	−0.28815	0.21009
FA-tuned PI [4]	4.8609	−0.30629	0.15649
GA-tuned PI [4]	5.915	−0.30174	0.17586

TABLE 7. Numerical results of *ST*, *US* and *OS* for Δf_2 under disturbance (b).

Approach	*ST* (*s*)	*US*	*OS*
RIME-tuned PI (proposed)	2.4666	**−0.22173**	**0.045868**
BWOA-tuned PI [1]	**2.4345**	−0.22176	0.069598
SSA-tuned PI [2]	2.6428	−0.25758	0.069851
SFLA-tuned PI [3]	10.284	−0.27376	0.21862
FA-tuned PI [4]	5.6082	−0.27569	0.13757
GA-tuned PI [4]	6.4615	−0.29459	0.14987

TABLE 8. Numerical results of *ST*, *US* and *OS* for ΔP_{tie} under disturbance (b).

Approach	*ST* (*s*)	*US*	*OS*
RIME-tuned PI (proposed)	**2.0045**	**−0.02955**	0.022888
BWOA-tuned PI [1]	2.0241	−0.033847	**0.022492**
SSA-tuned PI [2]	2.3188	−0.037899	0.03253
SFLA-tuned PI [3]	8.5521	−0.06469	0.045274
FA-tuned PI [4]	2.5018	−0.050536	0.036399
GA-tuned PI [4]	4.5398	−0.05461	0.045326

E. PERFORMANCE INDICES AND ROBUSTNESS

In addition to the adopted *OF*, three different objective functions (*IAE*, *ISE*, and *ITSE*) are also used to further measure the performance of the controllers employed in the AGC problem. The expressions for these objective functions are defined in (12) - (14).

$$IAE = \int_0^{30} (|\Delta f_1| + |\Delta f_2| + |\Delta P_{tie}|) \cdot dt \tag{12}$$

$$ISE = \int_0^{30} \left[(|\Delta f_1|)^2 + (|\Delta f_2|)^2 + (|\Delta P_{tie}|)^2\right] \cdot dt \tag{13}$$

$$ITSE = \int_0^{30} t \cdot \left[(|\Delta f_1|)^2 + (|\Delta f_2|)^2 + (|\Delta P_{tie}|)^2\right] \cdot dt \tag{14}$$

In this work, we consider a modified version of ITAE as the main *OF*. Although this modified ITAE is primarily used in research to analyze the performance of the proposed controller, its robustness in comparison to other objective functions must be evaluated. Tables 9 and 10 record the values of the four *OF*s for both disturbance scenarios (a) and (b). The results of a comprehensive analysis of Tables 9 and 10 highlight the superior performance of the RIME-tuned PI controller across various *OF*s. The controller consistently achieves lower values for IAE, ITAE, ISE, and ITSE, indicating its effectiveness in controlling the system subject to disturbances. The data from both disturbance scenarios supports the conclusion that the RIME-tuned PI controller outperforms other controllers across a wide range of objective functions, demonstrating its resilience and suitability for the AGC problem.

TABLE 9. Numerical results of performance indices under disturbance (a).

Approach	*IAE*	*ITAE*	*ISE*	*ITSE*
RIME-tuned PI (proposed)	**0.8236**	**3.0773**	**0.0559**	**0.0994**
BWOA-tuned PI [1]	0.9979	3.7909	0.0835	0.1531
SSA-tuned PI [2]	1.0240	3.4662	0.0970	0.1624
SFLA-tuned PI [3]	3.2445	23.7959	0.3903	1.6722
FA-tuned PI [4]	1.7207	7.4259	0.2097	0.4723
GA-tuned PI [4]	2.3341	12.1244	0.2802	0.8618

TABLE 10. Numerical results of performance indices under disturbance (b).

Approach	*IAE*	*ITAE*	*ISE*	*ITSE*
RIME-tuned PI (proposed)	**0.9051**	**2.9150**	**0.0772**	**0.1105**
BWOA-tuned PI [1]	0.9750	3.5131	0.0864	0.1318
SSA-tuned PI [2]	1.1754	4.9948	0.1224	0.1774
SFLA-tuned PI [3]	3.0593	21.5626	0.3529	1.3947
FA-tuned PI [4]	1.7667	7.3783	0.2215	0.4635
GA-tuned PI [4]	2.3784	11.8846	0.3060	0.8642

VI. CONCLUSION

AGC is crucial for enhancing the operational efficiency of power systems and ensuring a reliable and consistent energy supply to consumers. This study presents a hybrid power system comprising an reheat thermal power system and a PV system, in which AGC is implemented to manage the system's inherent dynamic issues. To control frequency oscillations and tie line power changes, a traditional PI controller is employed. The RIME optimization algorithm is utilized to optimize the parameters of the PI controller. This study represents the first use of RIME, a relatively new optimization technique, in the AGC process. An enhanced ITAE is used as the objective function in the optimization process, demonstrating a commitment to improving and developing control measures. A comprehensive study was conducted in various scenarios to assess the effectiveness of the RIME-tuned PI controller. The results were then compared to optimization techniques that have been proven successful in the literature, such as BWOA, SSA, SFLA, FA, and GA. The findings consistently demonstrate that the RIME algorithm outperforms its counterparts, making it more effective in optimizing PI controller parameters for the AGC process. The RIME-tuned PI controller outperforms the combined BWOA, SSA, SFLA, FA, and GA approaches in

reducing frequency oscillations and tie line power changes. The results indicate that a highly successful and efficient approach to AGC process in power systems is the RIME-tuned PI controller. The exceptional integration of the RIME algorithm into the AGC framework demonstrates its merit and ability to achieve outstanding system performance. This work validates the potential of the RIME method as a reliable tool for enhancing power system stability and dependability.

REFERENCES

[1] P. Dahiya and A. K. Saha, "Frequency regulation of interconnected power system using black widow optimization," *IEEE Access*, vol. 10, pp. 25219–25236, 2022, doi: 10.1109/ACCESS.2022.3155201.

[2] E. Çelik, N. Öztürk, and E. H. Houssein, "Influence of energy storage device on load frequency control of an interconnected dual-area thermal and solar photovoltaic power system," *Neural Comput. Appl.*, vol. 34, no. 22, pp. 20083–20099, Nov. 2022, doi: 10.1007/s00521-022-07558-x.

[3] R. K. Khadanga, A. Kumar, and S. Panda, "A hybrid shuffled frog-leaping and pattern search algorithm for load frequency controller design of a two-area system composing of PV grid and thermal generator," *Int. J. Numer. Model., Electron. Netw., Devices Fields*, vol. 33, no. 1, Jan. 2020, Art. no. e2694, doi: 10.1002/jnm.2694.

[4] S. M. Abd-Elazim and E. S. Ali, "Load frequency controller design of a two-area system composing of PV grid and thermal generator via firefly algorithm," *Neural Comput. Appl.*, vol. 30, no. 2, pp. 607–616, Jul. 2018, doi: 10.1007/s00521-016-2668-y.

[5] D. Mohanty and S. Panda, "Modified salp swarm algorithm-optimized fractional-order adaptive fuzzy PID controller for frequency regulation of hybrid power system with electric vehicle," *J. Control, Autom. Electr. Syst.*, vol. 32, no. 2, pp. 416–438, Apr. 2021, doi: 10.1007/s40313-020-00683-9.

[6] M. S. Alam, F. S. Al-Ismail, and M. A. Abido, "PV/Wind-integrated low-inertia system frequency control: PSO-optimized fractional-order PI-based SMES approach," *Sustainability*, vol. 13, no. 14, p. 7622, Jul. 2021, doi: 10.3390/su13147622.

[7] A. Elmelegi, E. A. Mohamed, M. Aly, E. M. Ahmed, A. A. Mohamed, and O. Elbaksawi, "Optimized tilt fractional order cooperative controllers for preserving frequency stability in renewable energy-based power systems," *IEEE Access*, vol. 9, pp. 8261–8277, 2021, doi: 10.1109/ACCESS.2021.3049782.

[8] V. Padiachy and U. Mehta, "Novel fractional-order proportional-integral controller for hybrid power system with solar grid and reheated thermal generator," *Solar*, vol. 3, no. 2, pp. 298–321, Jun. 2023, doi: 10.3390/solar3020018.

[9] A. E. Khalil, T. A. Boghdady, M. H. Alham, and D. K. Ibrahim, "Enhancing the conventional controllers for load frequency control of isolated microgrids using proposed multi-objective formulation via artificial rabbits optimization algorithm," *IEEE Access*, vol. 11, pp. 3472–3493, 2023, doi: 10.1109/ACCESS.2023.3234043.

[10] A. Daraz, S. A. Malik, A. Basit, S. Aslam, and G. Zhang, "Modified FOPID controller for frequency regulation of a hybrid interconnected system of conventional and renewable energy sources," *Fractal Fractional*, vol. 7, no. 1, p. 89, Jan. 2023, doi: 10.3390/fractalfract7010089.

[11] G. Sahoo, R. K. Sahu, S. Panda, N. R. Samal, and Y. Arya, "Modified Harris hawks optimization-based fractional-order fuzzy PID controller for frequency regulation of multi-micro-grid," *Arabian J. Sci. Eng.*, vol. 48, no. 11, pp. 14381–14405, Nov. 2023, doi: 10.1007/s13369-023-07613-2.

[12] D. Sibtain, T. Rafiq, M. H. Bhatti, S. Shahzad, and H. Kilic, "Frequency stabilization for interconnected renewable based power system using cascaded model predictive controller with fractional order PID controller," *IET Renew. Power Gener.*, vol. 17, no. 16, pp. 3836–3855, Dec. 2023, doi: 10.1049/rpg2.12885.

[13] A. M. Abdel-Hamed, A. Y. Abdelaziz, and A. El-Shahat, "Design of a 2DOF-PID control scheme for frequency/power regulation in a two-area power system using dragonfly algorithm with integral-based weighted goal objective," *Energies*, vol. 16, no. 1, p. 486, Jan. 2023, doi: 10.3390/en16010486.

[14] E. Çelik, "Design of new fractional order PI–fractional order PD cascade controller through dragonfly search algorithm for advanced load frequency control of power systems," *Soft Comput.*, vol. 25, no. 2, pp. 1193–1217, Jan. 2021, doi: 10.1007/s00500-020-05215-w.

[15] E. Çelik, N. Öztürk, Y. Arya, and C. Ocak, "(1 + PD)-PID cascade controller design for performance betterment of load frequency control in diverse electric power systems," *Neural Comput. Appl.*, vol. 33, no. 22, pp. 15433–15456, Nov. 2021, doi: 10.1007/s00521-021-06168-3.

[16] R. K. Khadanga, A. Kumar, and S. Panda, "A novel modified whale optimization algorithm for load frequency controller design of a two-area power system composing of PV grid and thermal generator," *Neural Comput. Appl.*, vol. 32, no. 12, pp. 8205–8216, Jun. 2020, doi: 10.1007/s00521-019-04321-7.

[17] P. J. Krishna, V. P. Meena, N. Patnana, A. Mathur, and V. P. Singh, "Grey wolf optimizer-assisted R-method-based weighted minimization for automatic generation control in two-area interconnected power system," *Int. J. Dyn. Control*, vol. 11, no. 4, pp. 1779–1796, Aug. 2023, doi: 10.1007/s40435-022-01070-9.

[18] S. Dewangan, T. Prakash, and V. Pratap Singh, "Design and performance analysis of elephant herding optimization based controller for load frequency control in thermal interconnected power system," *Optim. Control Appl. Methods*, vol. 42, no. 1, pp. 144–159, Jan. 2021, doi: 10.1002/oca.2666.

[19] S. P. Singh, T. Prakash, V. P. Singh, and M. G. Babu, "Analytic hierarchy process based automatic generation control of multi-area interconnected power system using Jaya algorithm," *Eng. Appl. Artif. Intell.*, vol. 60, pp. 35–44, Apr. 2017, doi: 10.1016/j.engappai.2017.01.008.

[20] A. Latif, S. M. S. Hussain, D. C. Das, and T. S. Ustun, "Optimization of two-stage IPD-(1+I) controllers for frequency regulation of sustainable energy based hybrid microgrid network," *Electronics*, vol. 10, no. 8, p. 919, Apr. 2021, doi: 10.3390/electronics10080919.

[21] S. Davtalab, B. Tousi, and D. Nazarpour, "Optimized intelligent coordinator for load frequency control in a two-area system with PV plant and thermal generator," *IETE J. Res.*, vol. 68, no. 5, pp. 3876–3886, Sep. 2022, doi: 10.1080/03772063.2020.1782777.

[22] M. Sharma, S. Prakash, S. Saxena, and S. Dhundhara, "Optimal fractional-order tilted-integral-derivative controller for frequency stabilization in hybrid power system using salp swarm algorithm," *Electr. Power Compon. Syst.*, vol. 48, no. 18, pp. 1912–1931, Nov. 2020, doi: 10.1080/15325008.2021.1906792.

[23] E. Sahin, "Design of an optimized fractional high order differential feedback controller for load frequency control of a multi-area multi-source power system with nonlinearity," *IEEE Access*, vol. 8, pp. 12327–12342, 2020, doi: 10.1109/ACCESS.2020.2966261.

[24] H. Su, D. Zhao, A. A. Heidari, L. Liu, X. Zhang, M. Mafarja, and H. Chen, "RIME: A physics-based optimization," *Neurocomputing*, vol. 532, pp. 183–214, May 2023, doi: 10.1016/j.neucom.2023.02.010.

[25] W. Zhu, L. Fang, X. Ye, M. Medani, and J. Escorcia-Gutierrez, "IDRM: Brain tumor image segmentation with boosted RIME optimization," *Comput. Biol. Med.*, vol. 166, Nov. 2023, Art. no. 107551, doi: 10.1016/j.compbiomed.2023.107551.

SERDAR EKINCI received the B.Sc. degree in control engineering and the M.Sc. and Ph.D. degrees in electrical engineering from Istanbul Technical University (ITU), in 2007, 2010, and 2015, respectively. He is currently an Associate Professor with the Department of Computer Engineering, Batman University, Turkey. His research interests include electrical power systems, stability, control technology, and the applications of metaheuristic optimization algorithms to various control systems.

ÖZAY CAN received the B.Sc., M.Sc., and Ph.D. degrees in electrical electronics engineering from Duzce University, in 2011, 2016, and 2022, respectively. He is currently an Assistant Professor with the Department of Electronics and Automation, Recep Tayyip Erdoğan University, Turkey. His research interests include power systems and control systems applications of metaheuristic optimization algorithms.

MUSTAFA ŞINASI AYAS (Member, IEEE) received the B.Sc.E. degree in electrical engineering from Hacettepe University, Ankara, Turkey, in 2009, and the M.Sc.E. and Ph.D. degrees in electrical engineering from Karadeniz Technical University (KTU), Trabzon, Turkey, in 2012 and 2017, respectively. He is currently an Associate Professor with the Department of Electrical and Electronics Engineering, KTU, and also a Visiting Scholar with the University of Tennessee, Knoxville, TN, USA. His research interests include automatic control systems, evolutionary optimization, robotic systems, secure control systems, and electric motor drive diagnostics.

DAVUT IZCI received the B.Sc. degree in electrical and electronic engineering from Dicle University, Turkey, and the M.Sc. and Ph.D. degrees in mechatronics and microsystems from Newcastle University, England, U.K. He is currently an Associate Professor working on optimization, control system design, sensing applications, energy harvesting, microsystems development and applications of metaheuristic optimization techniques to different control systems, and real-world engineering problems. He has published more than 100 articles in prestigious international journals. He is also a member of the editorial board in *e-prime* journal (Elsevier) and serves as a reviewer in several top tier journals in the field of metaheuristics, artificial intelligence, and control systems. He is recognized as one of the world's top 2% scientists by Elsevier and Stanford University.

MOHAMMAD SALMAN (Senior Member, IEEE) received the B.Sc., M.Sc., and Ph.D. degrees in electrical and electronic engineering from Eastern Mediterranean University (EMU) in 2006, 2007, and 2011, respectively. Currently, he is an Associate Professor with the Electrical Engineering Department, American University of the Middle East, Kuwait. With a prolific publication record, he has contributed to over 70 peer-reviewed journals and conference publications. His research interests include signal processing, adaptive filters, image processing, and sparse signal representation. Additionally, he has held various editorial and organizational roles, including a guest editor, the general chair, the program chair, and a TPC member, for numerous international journals and conferences.

MOSTAFA RASHDAN (Senior Member, IEEE) received the B.Sc. degree in electrical engineering and the M.Sc. degree in electronics and communications from Minia University, Egypt, in 1997 and 2001, respectively, and the Ph.D. degree in electrical and computer engineering from the University of Calgary, Alberta, Canada, in 2011. He was a Teaching Assistant with the High Institute of Energy, Aswan, Egypt, from 1999 to 2005. He was Postdoctoral Fellow with the RFIC Group, University of Calgary, from January 2011 to September 2011 and from July 2013 to January 2015. He was an Assistant Professor with the Faculty of Energy Engineering, Aswan University, Aswan, from September 2011 to June 2013. He is currently an Associate Professor with the American University of the Middle East, Kuwait. His current research interests include mixed signal integrated circuit design, time-based serial communication link architectures, and high-speed data converters. He has won several awards, such as the Outstanding Student IC Designer Award from Analog Devices Inc., in February 2013, and Kenneth C. Smith Early Career Award for Microelectronics Research from 43rd IEEE International Symposium on Multiple-Valued Logic (ISMVL 2013).